

# Theoretical analysis of heat pump assisted air gap membrane distillation

Martijn Bindels<sup>\*</sup>, Bart Nelemans

Aquastill, Nusterweg 69, 6136 KT Sittard, the Netherlands

## HIGHLIGHTS

- Three configurations for heat pump operation with V-AGMD are proposed.
- A configuration with constant membrane and condenser temperature shows great flux improvement.
- Slight changes to an existing model are made, making the results applicable for a real setup.
- Specific electrical energy consumption similar to mechanical vapour compression is possible.

## ARTICLE INFO

### Keywords:

Air gap membrane distillation  
Mechanical vapor compression  
Heat pump  
Modelling  
Zero liquid discharge (ZLD)

## ABSTRACT

Three configurations for heat pumps for simultaneously heating and cooling of vacuum assisted air gap membrane distillation (V-AGMD) are proposed and theoretically analysed. The benefit of using heat pumps is that local heating is not needed. The first configuration is the current state of the art a heat pump is used for the heating and cooling of V-AGMD. In the second configuration, a heat pump is connected to a V-AGMD module where the membrane and condenser channel have a constant temperature. The second configuration has a total distillate production of 3825 l/m<sup>2</sup>/h, but has a specific electrical energy consumption (SEEC) ranging between 16 and 107 kWh<sub>el</sub>/m<sup>3</sup>. The SEEC of the first configuration ranges between 9 and 22 kWh<sub>el</sub>/m<sup>3</sup>, which is higher than the thermodynamic limit. In the third configuration, a zero liquid discharge setup was proposed based on the first configuration. Results indicate that 26.7 kWh<sub>el</sub>/m<sup>3</sup> is needed to raise the 35 g/l feed water to 250 g/l, which is only slightly higher than the 25 kWh<sub>el</sub>/m<sup>3</sup> of mechanical vapour compression. Ammonia was used as a refrigerant in the calculations, making results applicable to real setups. In conclusion, heat pumps can provide heating and cooling, making them a promising solution.

## 1. Introduction

Membrane distillation (MD) is an upcoming desalination method where a vapour pressure difference across a semipermeable hydrophobic membrane is used to produce potable water [1]. In MD, the treated water does not have to reach the boiling point, which means that low grade heat can be used. For example, a marine engine's waste heat can be used for the production of fresh water [2,3]. Waste heat from power plants are another potential source of heat [4]. However, in some cases, waste heat might not be available, is limited in quantity (kw), low or variable in temperature, or the delivery of waste heat is intermittent [5]. Therefore, other heating methods are needed. Several heating methods have been proposed in literature. Solar membrane distillation has been researched in the past [6–12], but has geographical limitations. District heating can be used as a heat source, and was researched for the

treatment of flue gas condensate in cogeneration plants [13,14], and for the treatment of wastewater in the pharmaceutical industry [15]. Several new alternative methods have been researched, which are photothermal, electrothermal, microwave, and induction heating [16]. A less researched source of heating for membrane distillation are heat pumps (HP). A HP can be an option for MD, as they can provide heated water up to the temperatures needed for MD [17]. In a heat pump, a refrigerant undergoes two phase changes during the thermodynamic cycle, which is shown in Fig. 1. The refrigerant condenses in the condenser which provides the heating for MD. The refrigerant evaporates in the evaporator, which provides a cooling source. As MD needs both heating and cooling, the HP can also be used as cooling. Therefore, the HP provides simultaneous heating and cooling.

Normally, waste heat is used in membrane distillation. However, in some cases waste heat might not be available. For example, in solar

<sup>\*</sup> Corresponding author.

E-mail address: [m.bindels@aquastill.nl](mailto:m.bindels@aquastill.nl) (M. Bindels).

<https://doi.org/10.1016/j.desal.2021.115282>

Received 19 April 2021; Received in revised form 8 July 2021; Accepted 2 August 2021

Available online 6 August 2021

0011-9164/© 2021 Elsevier B.V. All rights reserved.

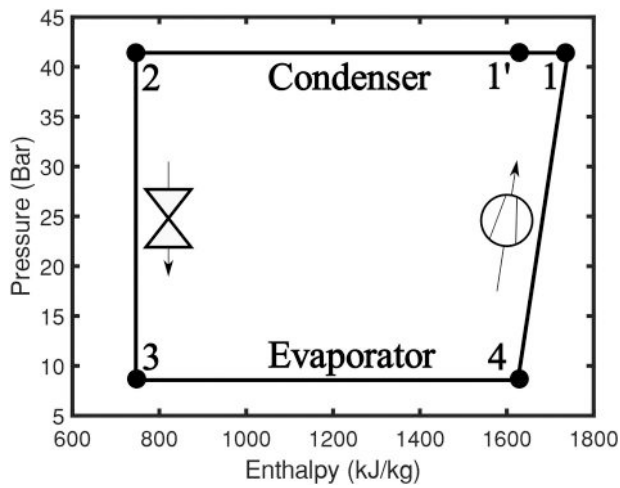


Fig. 1. Schematic view of thermodynamic cycle of a heat pump with a R717 ( $NH_3$ ) refrigerant.

membrane distillation solar collectors are used to provide heating for the process. However, solar heating has climate limitations. Therefore, the electricity grid can be used to provide heating via resistive heating. The problem with this is the high operational cost related to the electricity price. A heat pump can reduce the operating cost as less work is needed to provide the same amount of heating. Furthermore, the evaporator of the heat pump can be used as a cooling source, which reduces the size of the cooling tower if no cooling water is available. The increase in complexity of manufacturing and operation of a heat pump powered membrane system can therefore be justified by the reduction in energy use and application of MD in new locations.

To the authors' knowledge, only three articles [18–20] and one patent [21] was found which addresses the combination of a heat pump with membrane distillation. Tidiane Diaby et al. [19] proposed to use the condenser of an air conditioner for the heating of air gap membrane distillation (AGMD). The evaporator of the air conditioner was used for the cooling of the building. Please note that an air conditioner (AC) uses the same principles and components as a heat pump. The results from their study indicate that for a 24-storey building, more than  $14 \text{ m}^3$  could be made. Shaulsky et al. [18], proposed to combine direct contact membrane distillation with a heat pump and a heat exchanger. This study has several limitations. In the analysis Fluorochloroform (also known as R11 or CFC-11) was used in the calculations. However, R11 is being phased out under the Montreal protocol [22], and therefore the results are not applicable in practice. The simulations were based on a direct contact membrane distillation (DCMD) setup with heat recovery. In [20] a theoretical analysis was performed on integrated direct contact membrane distillation module and heat pump (DCMD-HP). They found that the production cost was 0.5 to 2 USD/ $\text{m}^3$ .

As Aquastill uses vacuum assisted membrane distillation (V-AGMD), which is more performant than AGMD [23], it is unclear what the performance will be. As a result, more work is needed to understand the impact of the combination of heat pumps with membrane distillation.

In this work, three configurations are proposed where heat pumps and vacuum assisted air gap membrane are combined. The first configuration consists of the current state of the art in membrane distillation where heating and cooling is provided by a heat pump. The MD module and heat pump are connected using heat exchangers. The second proposed configuration uses an MD module with a constant membrane and condenser temperature. The second configuration is not yet producible due to the high pressures of the refrigerant. The first configuration is possible but can be expensive due to the high cost of high temperature heat pump. Therefore, it must be studied first to understand the impacts of the use of a heat pump in membrane distillation.

Due to the aforementioned limitations, only theoretical analyses are done. For this, an already validated model is slightly changed to the new boundary conditions. The third configuration is to study the performance of a heat pump driven MD system (HPMD) applied to zero liquid discharge.

## 2. Theoretical backgrounds

A vapour compression cycle of a heat pump (HP) is shown in Fig. 1. Between point one and two the condenser is located where heat is transferred to the environment under a constant temperature. Between points two and three the expansion valve is located where the refrigerant evaporates due to the pressure difference between the condenser and evaporator. Heat is taken from the environment between point three and four in the evaporator. Between four and one the compressor compresses the refrigerant. Afterwards, the refrigerant condenses between one and two which completes the refrigerant cycle.

### 2.1. Membrane distillation setups

Before showing the proposed configurations, some information is given about the types of setups that can be used when heating or cooling is provided by a heat pump. All the possible setups are shown in Fig. 2.

Setup A is the current state of the art of MD. The distillate output can be increased when the vapour pressure difference across the semi-permeable hydrophobic membrane is increased. Therefore, Block B, C, and D try to achieve a higher temperature difference to improve the distillate production. In B, a constant condenser temperature is achieved. This is done by replacing the condenser channel by the evaporator of the heat pump. In C, the membrane channel temperature is constant over the module length. This is done by placing the condenser of the heat pump adjacent to the membrane channel. As a result, the heat from the HP can be transferred to the membrane channel. In D, both the temperature of the membrane and condenser channel of the MD module is constant. This can be achieved by placing the condenser of the HP adjacent to the membrane channel, and replacing the condenser channel of the MD module with the evaporator of the HP. It was found that setup B and C are not better than setup D. Due to the constant temperature at one side, the other temperature drops quickly to the constant temperature. This results in a small temperature difference between the membrane and the condenser channel, which in turn leads to a small or even negative flux. Therefore, they are not discussed in this work for brevity.

The temperatures of the channels are constant as the condensation and evaporation of the refrigerant are assumed to happen at a constant pressure. When the phase change of the refrigerant happens at a constant pressure, the refrigerant temperature is constant.

### 2.2. Heat pump cycle calculations

The amount of heating ( $\dot{Q}_{heat}$ ), cooling ( $\dot{Q}_{cool}$ ) and needed power input ( $P$ ) can be obtained by equation one to three.

$$\dot{Q}_{heat} = \dot{m}(h_1 - h_2) \quad (1)$$

$$\dot{Q}_{cool} = \dot{m}(h_4 - h_3) \quad (2)$$

$$P = \dot{Q}_{heat} - \dot{Q}_{cool} = \dot{m}(h_1 - h_4) \quad (3)$$

where  $h$  is the enthalpy, and  $\dot{m}$  is the mass flow of the refrigerant. MD requires as much heating as cooling. As can be seen in Fig. 1, the amount of heating provided by the heat pump is larger than the amount of cooling. Therefore, the extra energy can be used for other purposes, which can be determined by Eq. (4).

$$\dot{Q}_{extra} = \dot{m}(h_1 - h_{1'}) \quad (4)$$

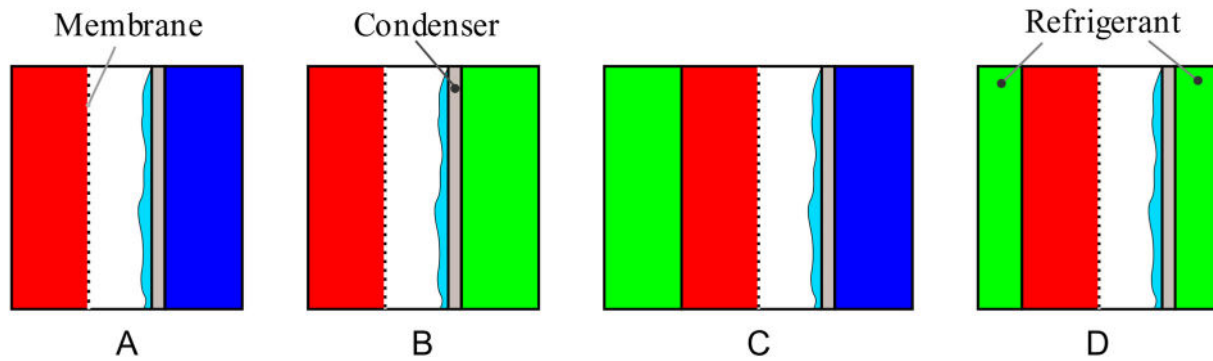


Fig. 2. Different possible setups when heating and/or cooling is provided by a heat pump. Red: hot brine, Blue: cold brine, and green: refrigerant. The dotted line is the membrane, the grey area next to the cold brine flow is the condenser foil.

If the distillate is removed from the system, a salinity increase will occur in the tank. As a result, fresh brine must be added to the system to keep the salinity constant. Heat pumps have a better COP when the temperature difference between the condenser and the evaporator are smaller. As MD shows the best performance at a membrane temperature of 80 °C, the condenser channel should be at an elevated temperature. Therefore, the fresh brine should be heated from its environmental temperature to the condenser channel temperature. This can be done with the extra energy of section 1-1'. As the evaporator of the heat pump needs to extract heat from its surrounding, the temperature of the surroundings must be warmer than the temperature of the evaporator. Therefore, the evaporator of the heat pump cannot be used for heating purposes even if its temperature is higher than the environment.

2.3. Proposed configurations

2.3.1. First configuration: current state of the art

The configuration of Fig. 3 is obtained when the current state of the art is used. The dotted line indicates the refrigerant stream, which has been given the same shape as the refrigerant cycle for clarification. As discussed earlier, the fresh brine should be preheated as the condenser channel of the MD module is at a higher temperature than the environment. Section 1-1' is used for heating the fresh brine. However, it might be possible that more heating is needed for brine heating than can be provided by the heat pump. Therefore, external heating is needed which can be provided by another heat pump, or by waste heat. Another

possibility is that enough extra heating is available to heat a secondary stage of MD, which can be cooled using external cooling water. As several heating sources are possible, the specific thermal energy consumption for the fresh brine heating is reported in the results.

2.3.2. Second configuration, constant membrane and condenser channel temperature

In this configuration, which is shown in Fig. 4, the membrane and the condenser channel of MD are constant. This is done by placing the condenser of the heat pump adjacent to the membrane channel. The cold channel of MD is replaced by the evaporator of the heat pump. In most cases, there is enough heating to provide heating for the fresh brine and to heat several secondary MD-stages. The secondary stages are conventional membrane distillation with external cooling. This way, the second stage does not need extra heating for the brine as the cooling can provide temperatures close to the environmental temperature).

2.3.3. Third configuration: minimal/zero liquid discharge

As stated earlier, the fresh brine should be heated. In the case when no brine is added, more heating can be used for the secondary stage. This leads to a minimal or zero liquid discharge system, shown in Fig. 5. The brine concentration will be done using a semi batch process, which means that the concentration rises during the process. The main and secondary stages are used to increase the concentration of the water in the tank. After the batch has concentrated to 250 g/l, it can be transported to a crystallizer in order to crystallize the remaining content of the

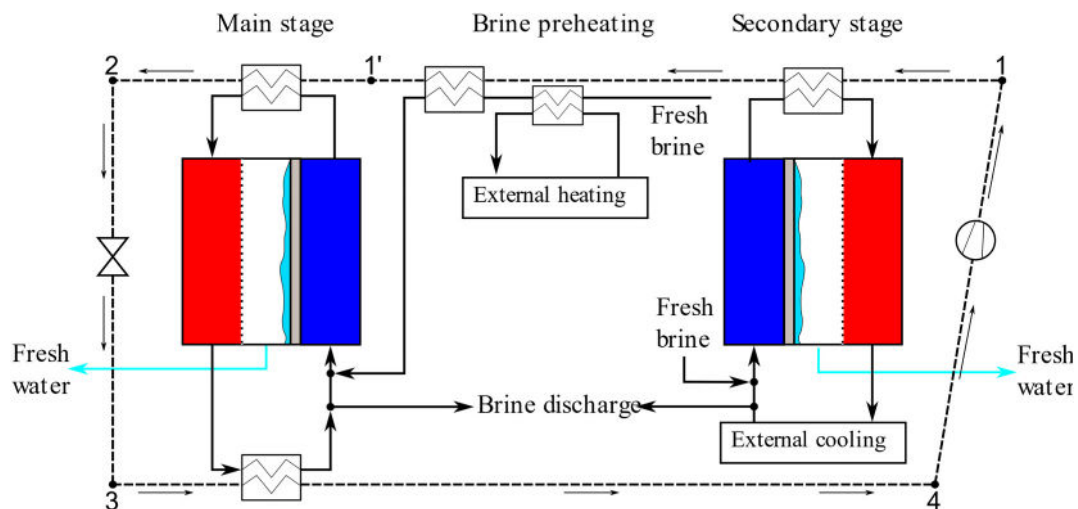


Fig. 3. Configurations where the state of the art is used. The dotted line is the refrigerant stream. The numbers correspond to the numbers shown in the refrigerant cycle. The arrows on the outside of the dotted line show the direction of the refrigerant. Brine is discharged and fresh brine is added to keep the salinity constant. The fresh water is transported out of the system.

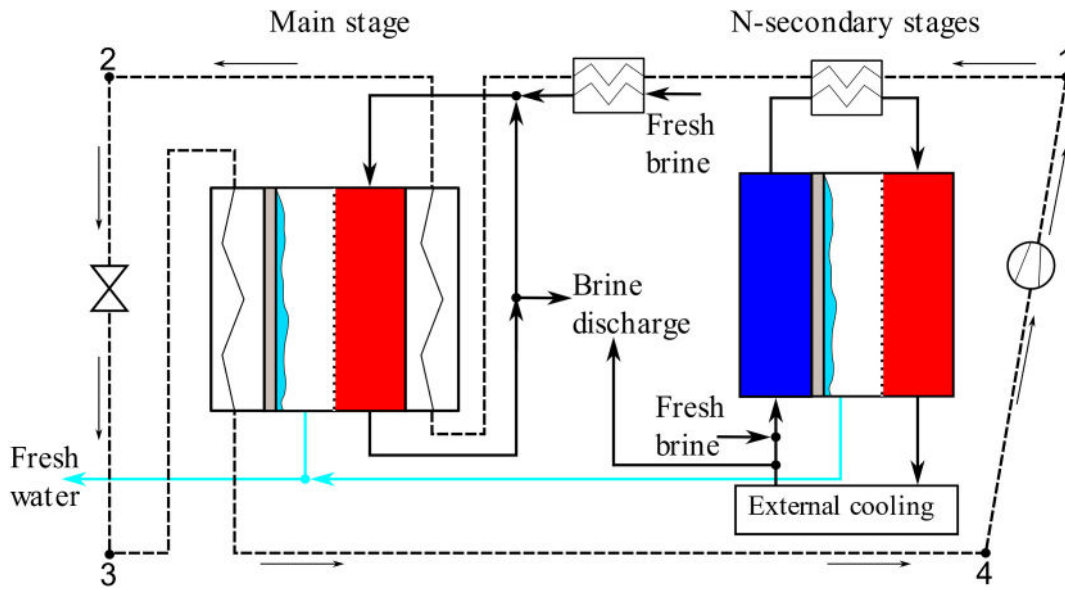


Fig. 4. Schematic presentation of the second configuration. Enough heating is available for the heating of the first and second stage, and for the heating of the fresh brine. The dotted line is the refrigerant stream. The numbers correspond to the numbers shown in the refrigerant cycle. The arrows on the outside of the dotted line show the direction of the refrigerant. Brine is discharged and fresh brine is added to keep the salinity constant. The fresh water is transported out of the system.

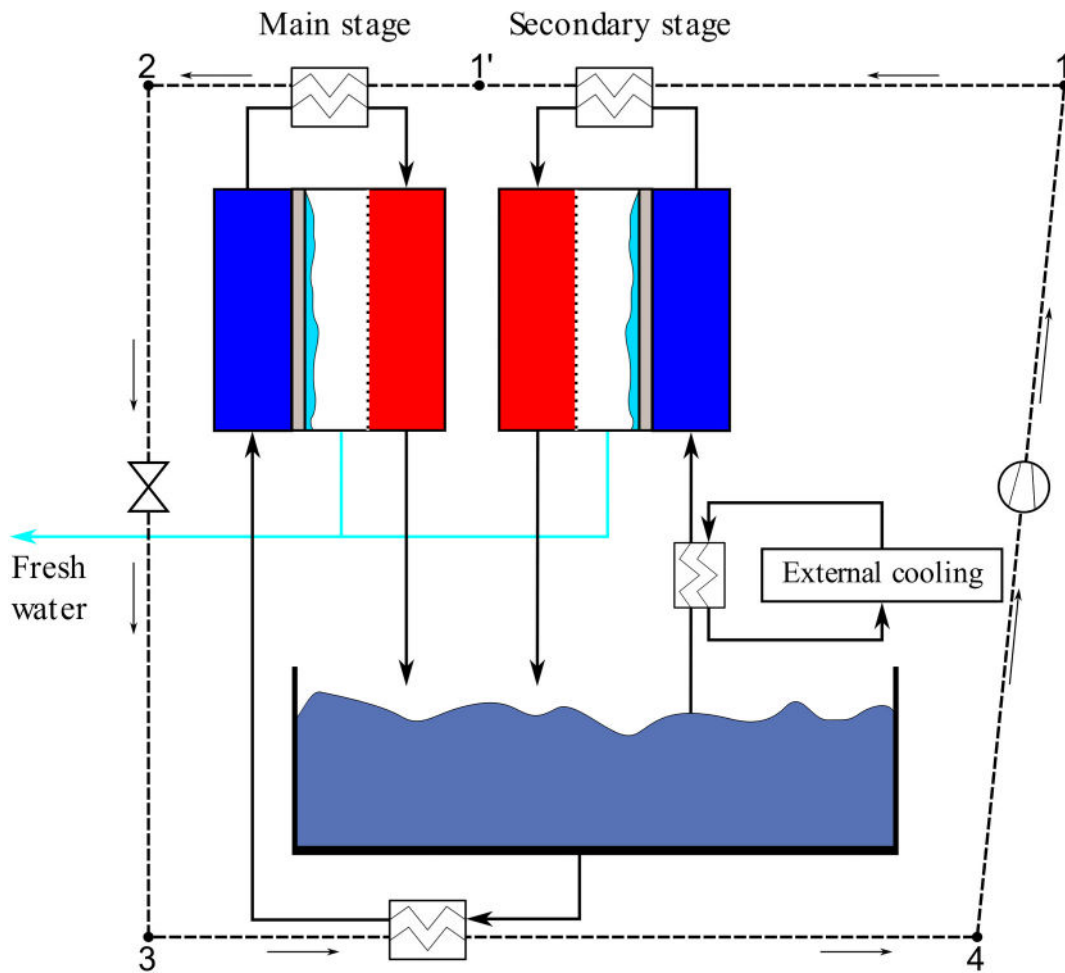


Fig. 5. Setup proposed for zero or minimal liquid discharge.

tank [24].

#### 2.4. Models of the configurations

The heat pump can be modelled by previously shown Eqs. (1) to (3). Currently, R717 or  $NH_3$  is used to provide heating to 90 °C with heat pumps [17]. Therefore, R717 was used as a refrigerant in the analyses. CoolProp [25] was used for obtaining the enthalpies of the refrigerant cycle. The models explained in the next section are based on an earlier validated model [26]. However, small changes are made to be able to simulate the second configuration. Therefore, the model and key equations from [26] are repeated here. The derivations are shown in the appendix. The model divides the envelope in 25 sections of equal temperature drop. Then for the length of each section is determined by Eq. (5). The term above the division is the amount of heat available in the slice. The term below the division is the heat lost in the slice. The temperature difference between the hot side of the membrane and the cold side of the airgap ( $\Delta T_{cal}$ ) is used to calculate the distillate flux.

$$L^i = \frac{v_H^m d_{h,sp} C_{p,sw}^i (T_{h,in}^i - T_{h,out}^i)}{J^i \Delta h_f^i + h_{m+a}^i \left( \Delta T_{cal}^i + \left( T_{ave}^i + C - \frac{B}{A - \ln(P_{sw}^i)} \right) \right)} \quad (5)$$

$$\Delta T_{cal}^i = \left( \frac{h_{fc}^i \ln(T_d^i) - J^i \Delta h_f^i}{h_{m+a}^i + h_{fc}^i} - \left( T_{ave}^i + C - \frac{B}{A - \ln(P_{sw}^i)} \right) + 3\Delta T_{est}^i \right) 0.25 \quad (6)$$

$$h_{fc}^i = \left( \frac{1}{h_{ch,h}^i} + \frac{1}{h_{con}^i} + \frac{1}{h_{ch,c}^i} \right)^{-1} \quad (7)$$

$\ln(T_d^i)$  is the logarithmic temperature difference between the two membrane and condenser channel, which will be changed to the another temperature difference in the second configuration.

##### 2.4.1. Model of configuration one: current state of the art

The model from [26] was used to simulate the MD part of this configuration. From a given membrane and condenser inlet temperature the rest of the parameters can be determined. Based on the heat exchanger effectiveness, the condenser and evaporator temperature of the heat pump can be determined. To reach a given membrane inlet temperature, the heat pump condenser must be higher than the given temperature as a temperature difference is needed for heat transfer. Eqs. (8) and (9) can be used to determine the heat exchanged in the heat exchanger. Combining Eqs. (8) and (9), results in Eq. (10), which can be used to calculate the temperature of the condenser of the HP. An effectiveness ( $\epsilon$ ) of 0.67 was used for all calculations. This value is equal to the effectiveness of current heat exchangers employed by Aquastill.

$$Q_{trans,1} = \epsilon \dot{m}_{brine,1} c_p (T_{HP,condenser} - T_{con,out,1}) \quad (8)$$

$$Q_{trans,1} = \dot{m}_{brine,1} c_p (T_{mem,in,1} - T_{con,out,1}) \quad (9)$$

$$T_{HP,condenser} = \frac{(T_{mem,in,1} - T_{con,out,1})}{\epsilon} + T_{con,out,1} \quad (10)$$

A similar process is done for the evaporator temperature, which should be slightly colder than the desired condenser inlet temperature. This results in Eq. (11).

$$T_{HP,evap} = T_{con,in,1} - \frac{(T_{mem,out,1} - T_{con,in,1})}{\epsilon} \quad (11)$$

Based on the temperatures and the vapour quality of the heat pump cycle, the enthalpies can be determined. The refrigerant mass flow can then be determined by Eq. (12). Based on the refrigerant mass flow, the supplied heating of the heat pump can be calculated.  $\dot{D}_{tot}$  is the total

production of the module in kg/s. The needed heating for brine can be calculated with Eq. (13), and the available heating of the heat pump can be computed with Eq. (14).

$$\dot{m} = \frac{\dot{Q}_{cool}}{h_4 - h_3} \quad (12)$$

$$\dot{Q}_{brine} = \dot{D}_{tot,stage 1} c_p (T_{con,in} - T_{\infty}) \quad (13)$$

$$\dot{Q}_{heat,HP} = \dot{m}(h_1 - h_2) \quad (14)$$

The extra heating needed can now be determined by Eq. (15). As previously stated, there is an extra heating source needed for fresh brine heating.

$$\dot{Q}_{heat,external} = \dot{Q}_{heat,HP} - \dot{Q}_{heat,MD} - \dot{Q}_{brine} \quad (15)$$

##### 2.4.2. Model of configuration two: constant condenser and membrane temperature

For this configuration, the model must be changed slightly. Instead of using the logarithmic temperature difference, which would result in a numerical error, the temperature difference is now the temperature difference between the cool and the hot side.

Furthermore, the length of the slice is normally calculated based on the length needed for a certain drop in brine temperature. As the temperatures are assumed to be constant, the length of the module is divided in to 25 equal sections.  $h_{fc}$  has been slightly to Eq. (16).

$$h_{fc}^i = \left( \frac{1}{h_{ch,h}^i} + \frac{1}{h_{con}^i} \right)^{-1} \quad (16)$$

As was introduced earlier, in some cases heating is available for another stage of membrane distillation. The heating value of this stage can be computed by Eq. (17). The MD model can then be used to find the correspondent mass flow to the thermal energy use. In the case that external heating is needed, it was calculated with Eq. (15).

$$\dot{Q}_{heat,stage 2} = \dot{Q}_{heat,HP} - \dot{Q}_{heat,MD} - \dot{Q}_{brine} \quad (17)$$

#### 2.5. Thermodynamic limit

The model in this works considers all effects that are relevant to the operation of membrane distillation. However, the thermodynamic limits of MD are not considered in the model. Therefore, the minimal specific electricity consumption is calculated here.

The SEEC is mostly influenced by the maximum COP of the heat pump (Eq. (18)).

$$COP = \frac{T_{HP,condenser}}{T_{HP,condenser} - T_{HP,evaporator}} = \frac{Q_H}{P_{in}} \quad (18)$$

It is clear from Eq. (18), that an increase in COP reduces the needed power input for the same amount of heating. Therefore, a lower SEEC is possible if the temperature difference between the hot and cold sink is minimal. However, the SEEC will hit a thermodynamic limit. For example, the limit for desalinating seawater with RO is 1.1 kWh/m<sup>3</sup> at 50% recovery [27].

The limit of MD can be calculated with Eq. (19) [28]. With the definition of GOR (Eq. (20)) and COP, the minimal SEEC can be calculated as Eq. (21). The factor of f is to convert from J to kWh. The COP is calculated by Eq. (22), which is the COP of a Carnot cycle.

$$GOR_{limit,MD} = \frac{T_{f,in} - T_{c,in}}{BPE_{f,in}} - 1 \quad (19)$$

$$GOR = \frac{h_{fg}}{Q_H} \quad (20)$$

$$SEEC_{min} = \frac{h_{fg, T_{f,in}}}{GOR \cdot COP_c \cdot f} \quad (21)$$

$$COP_c = \frac{T_{f,in}}{T_{f,in} - T_{c,in}} \quad (22)$$

The latent heat can be calculated at the membrane inlet temperature as most distillate will evaporate at a higher temperature. Using common temperatures of 80 °C and 20 °C for the membrane and condenser inlet results in a minimal SEEC of 4.45 kWh/m<sup>3</sup>, which is higher than the prementioned limit of RO. More discussion about the thermodynamic limits and its implications can be found in the [Results and discussion](#).

### 3. Methods

All simulations were done with a salinity of 35 g/kg, and an air gap pressure of 20 kPa. More information about the operation of the vacuum system in V-AGMD can be found in [23]. All the simulations were done with a membrane or condenser flow of 2 m<sup>3</sup>/h, or a crossflow velocity of 0.0737 m/s. The heat exchangers in the configurations are calculated with an effectiveness of 0.667, which corresponds to the heat exchangers used at Aquastill. The simulations were run according to the MD module specifications of an AS26 shown in [Tables 1 and 2](#). The AS26 has 12 envelopes with a length of 2.7 m.

For simulating inefficiencies in the heat pump an isentropic efficiency of 70% was used. This increases the enthalpy of the refrigerant after it passes the compressor, which can be calculated with Eq. (23). There are also inefficiencies in the other components of the heat pump. For example, flow through a duct is accompanied by a pressure drop. This results in higher pressure at the end of the condenser is lower pressure at the beginning of the condenser. The expansion valve is assumed to be an isenthalpic process, which might not be the case in a real heat pump. However, both effects and other inefficiencies are out of scope.

$$h_{1,real} = \frac{h_{1,isen} - h_4}{\eta_{isen}} + h_4 \quad (23)$$

The simulation of the third configuration were run at a membrane inlet temperature of 80 °C, a condenser inlet temperature of 20 °C, and a starting NaCl concentration of 35 g/kg and stopping at 250 g/kg. The feed flow rate and pressure in the air gap is equal to the previous simulations.

## 4. Results and discussion

In this section the simulation results for each configuration are presented. The gained output ratio (GOR) is normally used for operation with a low exergy source, like waste heat. As electricity is a high-exergy energy carrier, and can be used for more versatile purposes, it holds more economic value. Therefore, the use of GOR is omitted here and only the specific electrical energy consumption (SEEC) is shown.

### 4.1. Thermodynamic limits

As discussed in the theoretical background, the lowest SEEC possible is defined by the thermodynamics of the process. The thermodynamic limit is defined by using a perfect configuration, with a thermal efficiency of  $\eta = 1$ , and a heat pump with a COP equal to the Carnot cycle.

**Table 1**  
Channel specifications.

Parameter	Value
Channel spacer channel thickness (mm)	2.01
Channel spacer porosity	0.7814
Air gap spacer channel thickness (mm)	0.81
Air gap channel spacer porosity	0.9045

**Table 2**  
Membrane and module specifications.

Parameter	Value
Membrane pore radius (μm)	0.16
Membrane porosity	0.85
Envelope length (m)	2.7
Number of envelopes	12

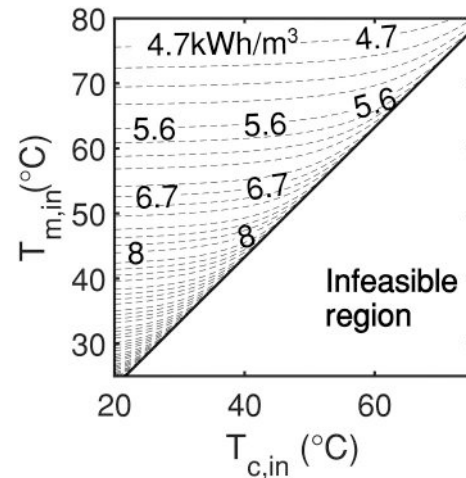


**Fig. 6.** Specific electrical energy consumption (SEEC) of a perfect MD system driven by heat pumps. The values shown in the figure are in kWh/m<sup>3</sup>. On the y-axis the membrane inlet temperature ranges from 25 to 80 °C, on the x-axis the condenser inlet temperature ranges from 20 to 75 °C. The bottom right of the graph is infeasible as the membrane inlet temperature cannot be higher than the condenser inlet temperature. All parameters were calculated at a salinity of 35 g/kg.

The results of such a system can be found in [Fig. 6](#). As can be seen, the location with the lowest possible SEEC is at a membrane and condenser inlet temperature of 80 °C and 20 °C, respectively. The minimal value was found to be 4.45 kWh/m<sup>3</sup>, which is higher than the reported practical minimum of RO [27]. Other reported values for RO are around the practical minimum [29,30]. Therefore, it can be stated that a HPMD system cannot beat seawater reverse osmosis (SWRO) based on electricity consumption. It should be noted that the choice for a certain desalination technology is not purely based on the SEEC alone. The COW of a HPMD system is based on the capital cost and the operational cost. When looking at the minimal kWh needed and using an electricity price of 0.15 USD/m<sup>3</sup> (which can even be higher when taxations are considered), the operating cost will be 0.70 USD/m<sup>3</sup>. For comparison, seawater reverse osmosis (SWRO) has reported unit cost between 0.5 USD/m<sup>3</sup> and 1.5 USD/m<sup>3</sup> [31].

In zero liquid discharge, the salinity of the treated brine increases during the process. The thermodynamic limit of the HPMD system can be seen. Also in the figure, the SEEC of mechanical vapour compression (MVC) and emerging RO-based processes for brine concentration are shown. These technologies are competitors of MD for ZLD. As the HPMD system also uses electricity, the comparison is valid.

### 4.2. Configuration one: current state of the art

The total distillate production of the whole configuration and flux of the main stage is shown in [Fig. 7](#). The y-axis and x-axis are the membrane and condenser inlet temperature, respectively. The temperatures shown in the figures are typical for a MD unit. As can be expected, the distillate flux of the main stage is highest at the highest membrane inlet temperature and lowest condenser inlet temperature. The MD system itself is not changed, which means that the flux of the main stage is

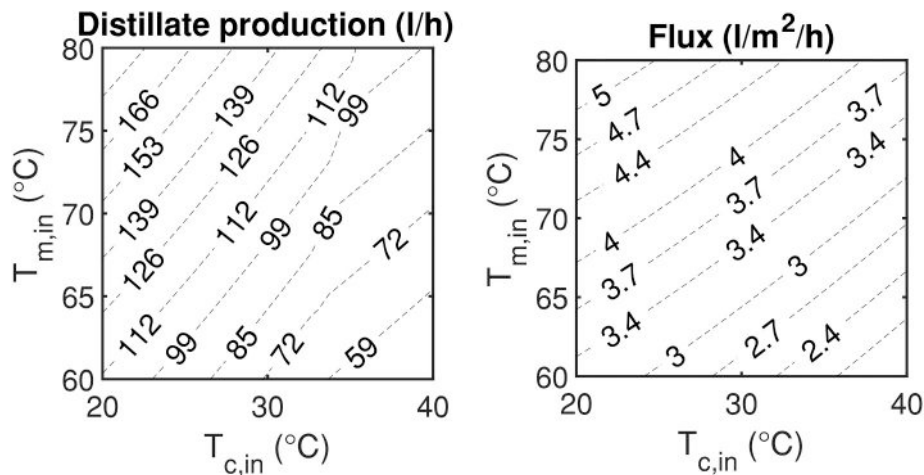


Fig. 7. Simulation results of the first configuration. Distillate production on the left and distillate flux of the main stage on the right. On the y-axis the membrane inlet temperature is shown, and on the x-axes the condenser inlet temperature of the main stage is shown.

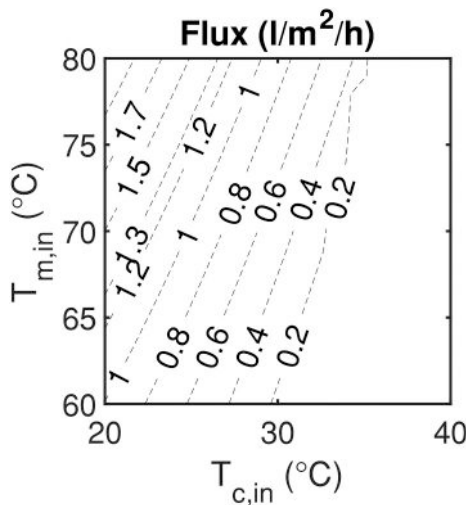


Fig. 8. Flux of the secondary stage. Please note that the condenser inlet shown on x-axis is the condenser inlet temperature of the main stage. The secondary stage has a condenser inlet temperature of 20 °C, so that brine heating is not needed for that stage. On the y-axis the membrane inlet temperature is shown, and on the x-axes the condenser inlet temperature of the main stage is shown.

comparable to what can be reached when MD is heated by low grade heat. In Fig. 8 the flux of the secondary stage is shown, which increases the total distillate production. As can be seen, the secondary stage only contributes for a small amount in the total distillate production. When the condenser inlet temperature is higher than 35 °C, all extra energy is needed for fresh brine preheating. The maximum distillate production reached with this configuration is 193 l/h.

In Fig. 9 the specific electrical energy consumption (SEEC) and specific thermal energy consumption (STEC) are shown. The lowest SEEC is 9 kWh/m<sup>3</sup> for this configuration, which is higher than the thermodynamic limit. Secondly, the SEEC required for this configuration is higher than the reported values of reverse osmosis [29,30]. As earlier mentioned, when the condenser inlet temperature is increased, all energy is needed for fresh brine heating. Even more, a small amount of thermal energy must be added to the system to preheat the fresh brine. However, the amount of extra heat required is still lower than what MD normally requires [32].

#### 4.3. Configuration two: constant membrane and condenser temperature

In this configuration both the membrane and condenser temperature of the main stage are constant. The results of this configuration are shown in Fig. 10. The total distillate production is high, mostly coming from the MD stage with a constant membrane and condenser temperature. The mean temperature difference from this configuration is higher than of the previous configuration, leading to an increase in distillate production. However, this leads to a higher energy use which results in a higher SEEC. The SEEC ranges from 16.3 to 107.2 kWh/m<sup>3</sup>. The maximum total distillate production is 3825 l/h.

The distillate production is high due to the number of secondary stages needed to satisfy the energy balance. The number of secondary stages and its distillate production are shown in Fig. 11. An increasing amount of stages results in a higher complexity of the system. As more stages are needed when the condenser inlet temperatures are lower, condenser temperatures below 40 °C are omitted. Furthermore, the SEEC decreases when the condenser inlet temperature increases.

The SEEC for this case are shown in Fig. 12, which is higher than the current state of the art. Due to the higher temperature difference between both sides of the membrane more heat is lost due to conduction. In the current state of the art the membrane module acts as a heat exchanger where the heat lost in the membrane channel is used for the heating of the condenser channel. In the second configuration, this is not possible resulting in a high thermal energy consumption, which in turn leads to a high SEEC. However, the total distillate production is higher. Therefore, this is a trade-off between capital cost and operational cost, which is out of scope of this work. There is only a small section of temperatures where extra heat should be applied to preheat the fresh brine.

As can be seen in Fig. 13, the distillate flux slowly reduces over the envelope length. This is due to reduction in membrane flow as distillate evaporates from the membrane channel. The reduction in flow reduces the heat transfer coefficient of the membrane channel, which reduces the temperature of the membrane-brine interface. Moreover, the salinity of the membrane channel increases, which reduces the water activity and distillate flux.

This configuration is not yet applicable due to the added complexity. With the current state of the art, five inlets or outlets are needed. For this configuration a total of seven inlets or outlets are needed. Furthermore, due to the high pressures of the refrigerant cycle, spiral wound modules are not possible. Hollow fibres can be used where the refrigerant is circulated in metal piping. However, using hollow fibre modules increases the complexity even more.



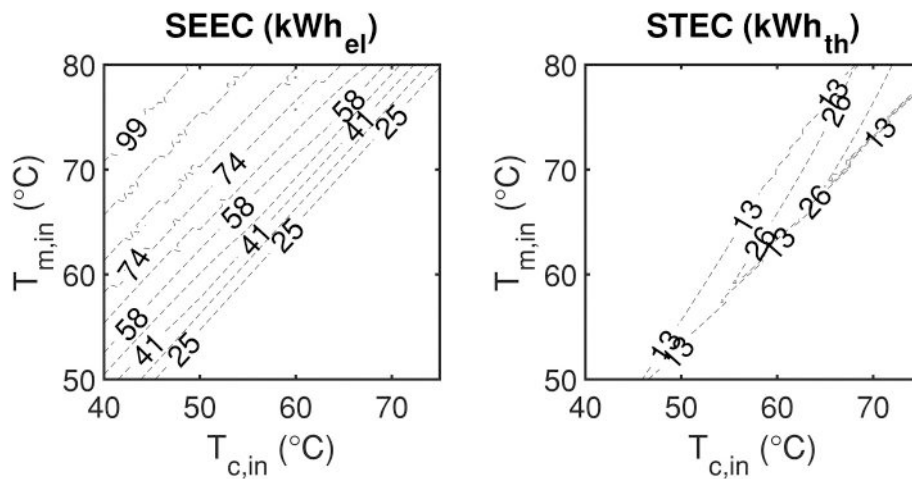


Fig. 12. Results of the second configuration. SEEC on the left and STEC on the right. On the y-axis the membrane inlet temperature is shown, and on the x-axes the condenser inlet temperature of the main stage is shown. No results exist for the bottom right corners as this region is infeasible.

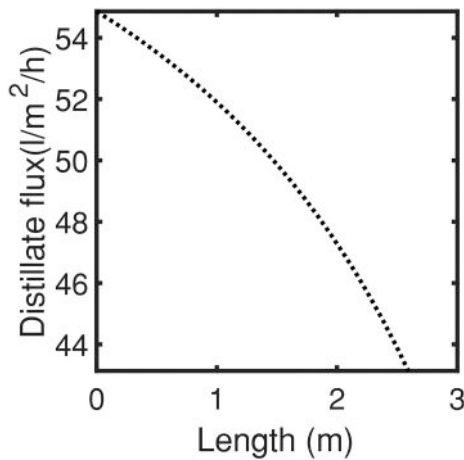


Fig. 13. Distillate flux for a module where both the membrane and condenser temperature are constant.

4.4. Effect of heat exchanger effectiveness

To study the effect of the heat exchanger effectiveness another simulation was done where the heat exchangers have an effectiveness of 1, which is a heat exchanger with infinite length. In Fig. 14 the change in SEEC and STEC are shown. A negative  $\Delta SEEC$  indicates that the SEEC is lower for a system with an effectiveness of 1 than for a system with an effectiveness of 0.67. As can be seen, the SEEC is lower while the STEC is higher. In an infinite length heat exchanger, the condenser temperature of the heat pump is lower. Furthermore, the evaporator temperature of the heat pump can be increased when perfect heat exchangers are used. Both effects results in a smaller temperature difference between the condenser and evaporator of the heat pump, which increase the COP. The increase in COP reduces the amount of extra heating, which increases the STEC as more external heating is needed to heat up the fresh brine. The change in distillate flux of the main stage was the same, while the flux of the secondary stage only changes by  $-0.1 \text{ l/m}^2/\text{h}$  and is therefore not shown in a graph.

4.5. Effect of isentropic efficiency of the compressor

In the previous analyses the isentropic efficiency of the compression was assumed to be 70%. To study the effect of the isentropic efficiency, a

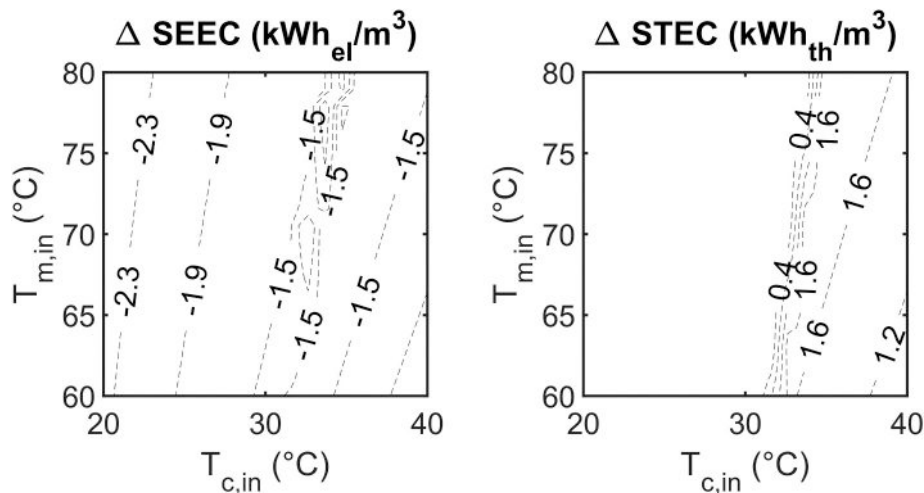


Fig. 14. Results of the first configuration with heat exchangers, SEEC is shown on the left and STEC is shown on the right.  $\Delta SEEC = SEEC_{\epsilon=1} - SEEC_{\epsilon=0.7}$ ,  $\Delta STEC = STEC_{\epsilon=1} - STEC_{\epsilon=0.7}$ .

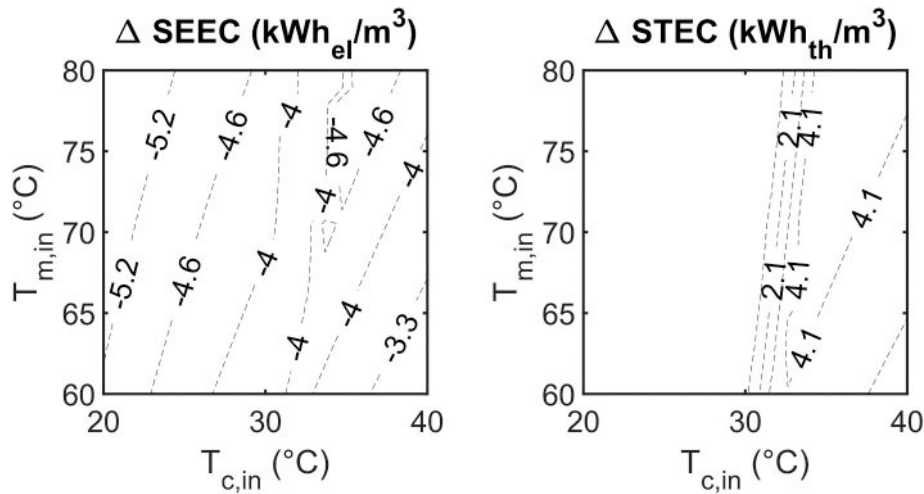


Fig. 15. Results of the first configuration showing the difference between the isentropic case.  $\Delta SEEC = SEEC_{\eta_{isen}=1} - SEEC_{\eta_{isen}=0.7}$ ,  $\Delta STEC = STEC_{\eta_{isen}=1} - STEC_{\eta_{isen}=0.7}$ .

new simulation was run where the compression is assumed to be isentropic. This only influenced the SEEC and STEC, so those two graphs are only shown here.

In Fig. 15, the difference between the isentropic and non-isentropic case can be seen. In the isentropic case the SEEC is lower ( $-2.7$  to  $-5.87$   $\text{kWh}_{el}/\text{m}^3$ ) and the STEC is higher (zero to  $+5.1$   $\text{kWh}_{th}/\text{m}^3$ ). The SEEC decreases as less power is needed in the compressor, or in other words, less losses are present in the compression. However, the losses result in a higher temperature which could be used for heating the fresh brine. This can also be seen in the change in the distillate flux of the secondary stage, shown in Fig. 16, which is lower than in a nonideal situation.

In this scenario, the lowest SEEC was found to be  $6.31$   $\text{kWh}_{el}/\text{m}^3$ , which is only slightly higher than the thermodynamic minimum. It can be stated that the isentropic efficiency of the heat pump is of more importance than the heat exchanger effectiveness.

#### 4.6. Configuration three: zero liquid discharge

In Fig. 17 the concentration of the brine and flux of the main and secondary stage can be seen during the process. The distillate flux of the main stage decreases due to the salinity increase that not only lowers the vapour pressure, but also the heat transfer of the channels. The flux of

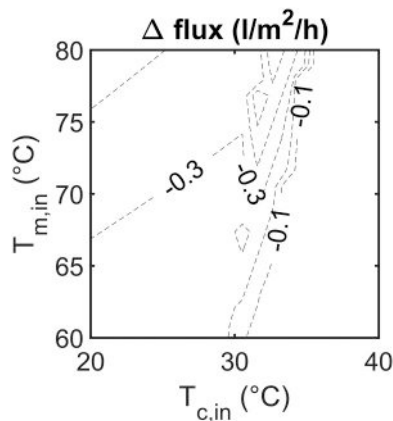


Fig. 16. Difference between isentropic compression and non-isentropic compression on the distillate flux of the secondary stage. A negative value means that the distillate flux of the secondary stage is lower in an ideal scenario compared to a nonideal scenario.

the secondary stage also decreases but with a smaller slope. This is due to the extra heating available as the main stage needs more electrical energy, and more heating is available for the secondary stage.

In Fig. 18, the electrical power consumption of the HPMD system is shown. More energy is needed during the process due to the change in thermophysical properties. The SEEC of this system is  $26.65$   $\text{kWh}/\text{m}^3$ . The size of the tank did not influence the SEEC.

Increasing the condenser inlet temperature to  $30$   $^{\circ}\text{C}$ , will reduce the energy consumption of the MD process. Before the operation of the HP can start, the fresh seawater must be heated to  $30$   $^{\circ}\text{C}$ . The trend of the graphs at  $30$   $^{\circ}\text{C}$  condenser inlet temperature is similar to  $20$   $^{\circ}\text{C}$  and therefore not shown. The results at  $30$   $^{\circ}\text{C}$  are compared with  $20$   $^{\circ}\text{C}$  in Table 3. There is less electrical energy needed when the condenser temperature is increased. However, the seawater is originally to be assumed at  $20$   $^{\circ}\text{C}$ . Before the HPMD can be started the seawater in the tank should be heated to  $30$   $^{\circ}\text{C}$ . This results in a thermal energy demand that can be accomplished by waste heat or by electrical heating (resistive heating or another smaller heat pump).

The SEEC of other proposed solutions for zero liquid discharge can be found in Table 4. In the work of Atia et al. [33] the SEEC was given for LSRRO, COMRO and OARO. Based on their results, a lower starting concentration and lower recovery reduces the SEEC. For LSRRO, the SEEC was  $3.4$   $\text{kWh}/\text{m}^3$  at a feed concentration of  $20$   $\text{g}/\text{l}$  and a recovery of  $85\%$ . However, the SEEC was  $68.3$   $\text{kWh}/\text{m}^3$  for a feed concentration of  $125$   $\text{g}/\text{l}$  and a recovery of  $50\%$ .

Compared to the SEEC of this work to the SEEC from other technologies, the RO based technologies are better performing in terms of energy consumption. Two stage MVC is only  $2.7$   $\text{kWh}/\text{m}^3$  higher, therefore, the ZLD HPMD system proposed here can compete with MVC in terms of electricity consumption.

## 5. Conclusions

In this work, three configurations of heat pumps with vacuum assisted air gap membrane distillation (V-AGMD) are presented. As heat pumps provide more heating than cooling in the same cycle, the extra heating was used to heat the fresh brine. The fresh brine should be added as not adding it would result in a concentration increase. The thermodynamic limit of a heat powered membrane distillate system is  $4.45$   $\text{kWh}/\text{m}^3$  at a membrane and condenser temperature of  $80$   $^{\circ}\text{C}$  and  $20$   $^{\circ}\text{C}$  respectively. All reported specific electrical energy consumption (SEEC) is higher than this value.

The first is the current state of the art where the heat pump provides heating and cooling via a heat exchanger. The specific electrical energy

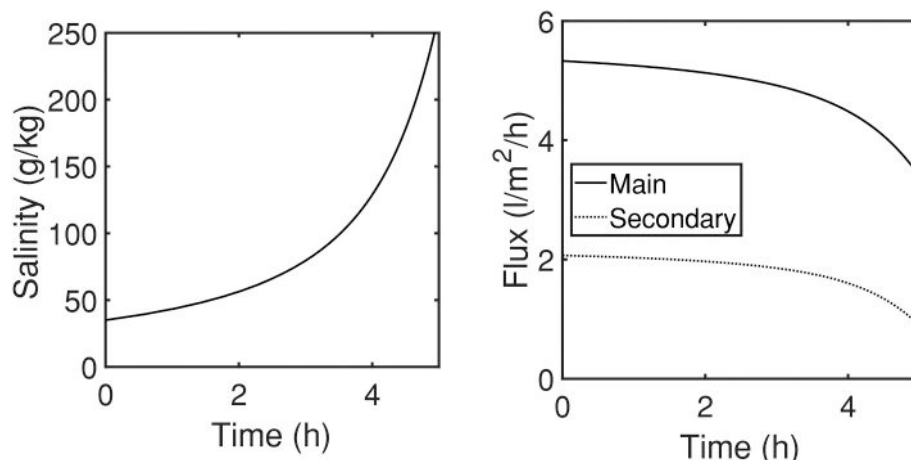


Fig. 17. Salinity of brine and distillate flux during the semi batch process. Begin volume and concentration are 1 m<sup>3</sup> and 35 g/kg. End concentration is 250 g/kg. Membrane and condenser inlet temperatures are 20 and 80 °C, respectively.

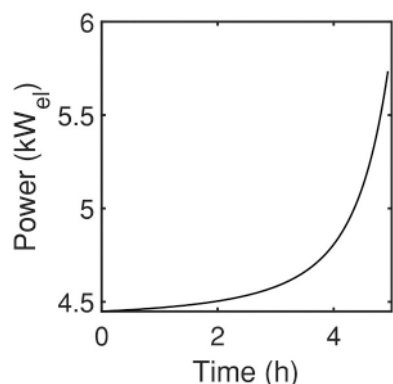


Fig. 18. Electrical power required for operation of semi batch HPMD.

Table 3

Energy needed for ZLD at 20 °C and 30 °C. Electrical energy needed for brine concentration is used by the HPMD system. At 30 °C the seawater should be heated first as it is originally assumed to be at 20 °C.

Condenser temperature (°C)	Electrical energy needed for brine concentration (kWh <sub>el</sub> /m <sup>3</sup> )	(Thermal) energy needed for heating the seawater tank to the condenser temperature (kWh <sub>th</sub> /m <sup>3</sup> )
20	26.65	0
30	21.42	11.11

Table 4

Specific electrical energy consumption (SEEC) of other proposed desalination technologies for brine concentration.

Technology	SEEC (kWh/m <sup>3</sup> )	Reference
Two stages mechanical vapour compression (MVC)	24 kWh/m <sup>3</sup> at 250 g/l	[34]
Two stage high pressure reverse osmosis (HPRO)	7.3 kWh/m <sup>3</sup> at 250 g/l	[34]
Four stage low-salt-rejection reverse osmosis (LSRRO).	5.2 kWh/m <sup>3</sup> from 0.6 M saline feed to 4 M brine concentration.	[35]

consumption (SEEC) of the first configuration is between 9 and 22 kWh<sub>el</sub>/m<sup>3</sup> which is higher than RO. However, due to the fresh brine heating an extra source of heating of 3 to 10 kWh<sub>th</sub>/m<sup>3</sup> is needed. The distillate flux of the first configuration is similar to what can be reached with using low-grade heating.

The second configuration shows more potential, as a total distillate production of more than 2000 l/h can be achieved. However, the SEEC ranges from 16.3 to 107.2 kWh<sub>el</sub>/m<sup>3</sup>, which is higher than when the heat pump is applied to the current state of the art. This setup can currently not yet be developed as added complexity of module production limits the practical employment of the configurations. Furthermore, the number of secondary stages needed increases the complexity of the setup.

In the third configuration a zero liquid discharge setup was proposed based on the first configuration. The SEEC of such a system is 26.65 kWh/m<sup>3</sup>, which is slightly higher than the 25 kWh/m<sup>3</sup> needed for mechanical vapour compression. Increasing the condenser inlet temperature decreases the SEEC. However, 11.11 kWh/m<sup>3</sup> of thermal energy is needed as the seawater must be heated from the environmental temperature (20 °C) up to the condenser inlet temperature (30 °C).

The effect of the non-isentropic compression was considered in the simulations. It was found that an isentropic process delivers lower SEEC than in the case of a non-isentropic compression. Considering an isentropic efficiency of 70% slightly increases the SEEC by 1 to 3.5 kWh/m<sup>3</sup> compared to an isentropic system. The effectiveness of the heat exchanger is considered in the simulations. An extra simulation was done to simulate the effect of the heat exchanger effectiveness. The total distillate SEEC decreases when the heat exchangers have an effectiveness of one. Therefore, a heat exchanger with a higher effectiveness improves the performance of the configurations. However, the beneficial effect is small.

To conclude, the use of heat pumps is promising for applications where local heating or cooling is not available.

**CRedit authorship contribution statement**

- Conceptualization: Martijn Bindels, Bart Nelemans
- Methodology: Martijn Bindels
- Software: Martijn Bindels
- Validation: Martijn Bindels
- Formal analysis: Martijn Bindels
- Investigation: Martijn Bindels
- Resources: Bart Nelemans
- Data Curation: Martijn Bindels
- Writing - Original Draft: Martijn Bindels
- Writing - Review & Editing: Bart Nelemans
- Visualization: Martijn Bindels
- Supervision: Bart Nelemans
- Project administration: Bart Nelemans
- Funding acquisition: Bart Nelemans

**Declaration of competing interest**

interests or personal relationships that could have appeared to influence the work reported in this paper.

The authors declare that they have no known competing financial

**Appendix A**

In Fig. 19 the temperature profile of the module is shown.

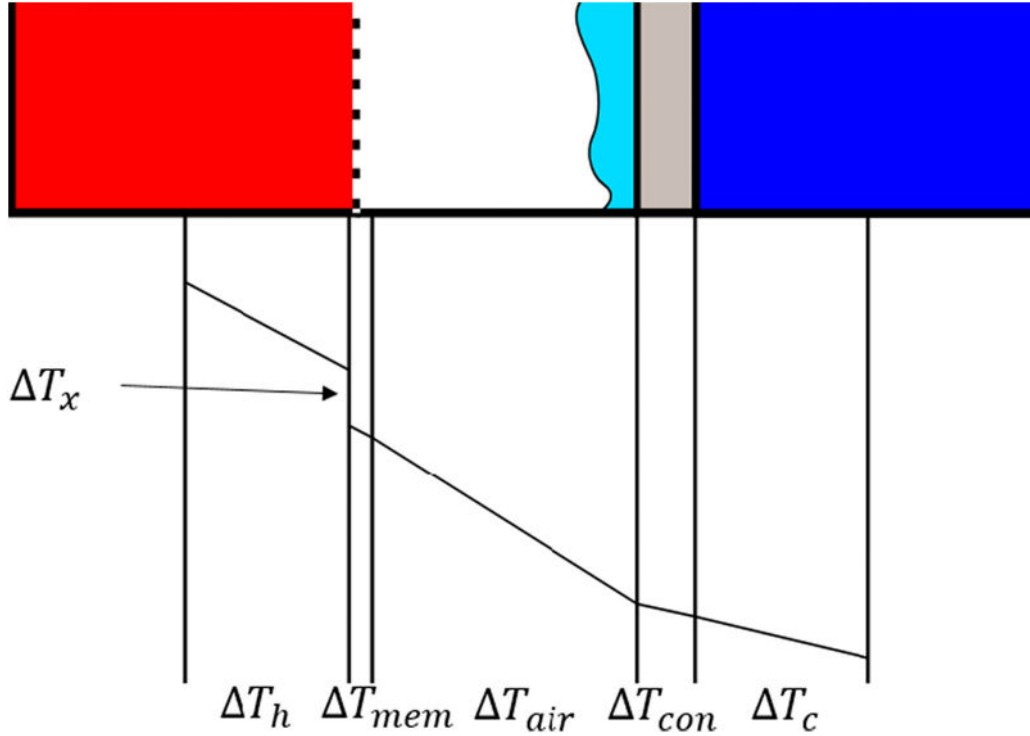


Fig. 19. Temperature profile of the MD unit.

The total temperature drop is equal to:

$$\Delta T_{in} = \Delta T_h + \Delta T_x + \Delta T_{mem} + \Delta T_{air} + \Delta T_{con} + \Delta T_c \tag{24}$$

$$\Delta T_{in} - \Delta T_x = \Delta T_{cal} + \Delta T_h + \Delta T_c + \Delta T_{con} \tag{25}$$

$$\Delta T_{in} - \Delta T_x = \Delta T_{cal} + \Delta T_h \left( 1 + \frac{h_h}{h_c} + \frac{h_1}{h_c} \right) \tag{26}$$

$\Delta T_h$  can be calculated with:

$$\Delta T_h = \frac{J^i h_f^i + h_{m+a}^i (\Delta T_{cal} + \Delta T_x)}{h_h} \tag{27}$$

Which can be used for further calculation:

$$\Delta T_{in} - \Delta T_x = \Delta T_{cal} + \frac{J^i h_f^i + h_{m+a}^i (\Delta T_{cal} + \Delta T_x)}{\left( \frac{1}{h_h} + \frac{1}{h_c} + \frac{1}{h_{con}} \right)^{-1}} \tag{28}$$

where the term under the division is equal to  $h_{fc}$ . Further rearranging leads to:

$$\Delta T_{cal} = \frac{(h_{cf} \Delta T_{in} - J^i h_f^i)}{h_{cf} + h_{m+a}} + \Delta T_x \tag{29}$$

As the equation changes when the distillate flux changes, extra term are added from the estimation of  $\Delta T_{cal}$  which is called  $\Delta T_{est}$ . This leads to:

$$\Delta T_{cal}^i = \left( \frac{h_{fc}^i \ln(T_d^i) - J^i \Delta h_f^i}{h_{m+a}^i + h_{fc}^i} - \left( T_{av}^i + C - \frac{B}{A - \ln(P_{sw}^i)} \right) + 3\Delta T_{est}^i \right) 0.25 \tag{30}$$

$\Delta T_x$  is to take temperature polarization into account, and assumes that the distillate evaporates in the air gap:

$$P_w = \exp\left(A - \frac{B}{T_{ave} - C}\right) a_w \quad (31)$$

When the distillate evaporates at a temperature of  $T_{ave}$ , the following equation can be used to approximate the temperature polarization:

$$T_{pol} = -C + \frac{B}{A - \ln(P_w)} \quad (32)$$

This leads to:

$$\Delta T_x = T_{pol} - T_{ave} \quad (33)$$

## References

- [1] A. Alkudhri, N. Darwish, N. Hilal, Membrane distillation: a comprehensive review, *Desalination* 287 (2012) 2–18, <https://doi.org/10.1016/j.desal.2011.08.027>.
- [2] R. Bahar, K.C. Ng, Fresh water production by membrane distillation (MD) using marine engine's waste heat, *Sustain. Energy Technol. Assess.* 42 (2020), 100860, <https://doi.org/10.1016/j.seta.2020.100860>.
- [3] Y. Xu, B.K. Zhu, Y.Y. Xu, Pilot test of vacuum membrane distillation for seawater desalination on a ship, *Desalination* 189 (2006) 165–169, <https://doi.org/10.1016/j.desal.2005.06.024>.
- [4] N. Dow, S. Gray, J. de Li, J. Zhang, E. Ostarcevic, A. Liubinas, P. Atherton, G. Roeszler, A. Gibbs, M. Duke, Pilot trial of membrane distillation driven by low grade waste heat: membrane fouling and energy assessment, *Desalination* 391 (2016) 30–42, <https://doi.org/10.1016/j.desal.2016.01.023>.
- [5] R.D. Gustafson, S.R. Hiibel, A.E. Childress, Membrane distillation driven by intermittent and variable-temperature waste heat: system arrangements for water production and heat storage, *Desalination* 448 (2018) 49–59, <https://doi.org/10.1016/j.desal.2018.09.017>.
- [6] A.E. Kabeel, M. Abdelgaied, E.M.S. El-Said, Study of a solar-driven membrane distillation system: evaporative cooling effect on performance enhancement, *Renew. Energy* 106 (2017) 192–200, <https://doi.org/10.1016/j.renene.2017.01.030>.
- [7] H. Chang, G.-B. Wang, Y.-H. Chen, C.-C. Li, C.-L. Chang, Modeling and optimization of a solar driven membrane distillation desalination system, *Renew. Energy* 35 (2010) 2714–2722, <https://doi.org/10.1016/j.renene.2010.04.020>.
- [8] P. Bendevis, A. Karam, T.M. Laleg-Kirati, Optimal model-free control of solar thermal membrane distillation system, *Comput. Chem. Eng.* 133 (2020), 106622, <https://doi.org/10.1016/j.compchemeng.2019.106622>.
- [9] J.D. Gil, J.D. Álvarez, L. Roca, J.A. Sánchez-Molina, M. Berenguel, F. Rodríguez, Optimal thermal energy management of a distributed energy system comprising a solar membrane distillation plant and a greenhouse, *Energy Convers. Manag.* 198 (2019), 111791, <https://doi.org/10.1016/j.enconman.2019.111791>.
- [10] E. Guillén-Burrieza, D.C. Alarcón-Padilla, P. Palenzuela, G. Zaragoza, Techno-economic assessment of a pilot-scale plant for solar desalination based on existing plate and frame MD technology, *Desalination* 374 (2015) 70–80, <https://doi.org/10.1016/j.desal.2015.07.014>.
- [11] J.D. Gil, L. Roca, A. Ruiz-Aguirre, G. Zaragoza, M. Berenguel, Optimal operation of a solar membrane distillation pilot plant via nonlinear model predictive control, *Comput. Chem. Eng.* 109 (2018) 151–165, <https://doi.org/10.1016/j.compchemeng.2017.11.012>.
- [12] A. Ruiz-Aguirre, M.I. Polo-López, P. Fernández-Ibáñez, G. Zaragoza, Assessing the validity of solar membrane distillation for disinfection of contaminated water, *Desalin. Water Treat.* 55 (2015) 2792–2799, <https://doi.org/10.1080/19443994.2014.946717>.
- [13] I.E.-. Noor, A. Martin, O. Dahl, District heating driven membrane distillation for advanced flue gas condensate treatment in combined heat and power plants, *J. Clean. Prod.* 292 (2021), 125979, <https://doi.org/10.1016/j.jclepro.2021.125979>.
- [14] A. Kullab, A. Martin, Membrane distillation and applications for water purification in thermal cogeneration plants, *Sep. Purif. Technol.* 76 (2011) 231–237, <https://doi.org/10.1016/j.seppur.2010.09.028>.
- [15] D.M. Woldemariam, A. Kullab, A.R. Martin, District heat-driven water purification via membrane distillation: new possibilities for applications in pharmaceutical industries, *Ind. Eng. Chem. Res.* 56 (2017) 2540–2548, <https://doi.org/10.1021/acs.iecr.6b04740>.
- [16] F.E. Ahmed, B.S. Lalia, R. Hashaikh, N. Hilal, Alternative heating techniques in membrane distillation: a review, *Desalination* 496 (2020), 114713, <https://doi.org/10.1016/j.desal.2020.114713>.
- [17] C. Arpagaus, F. Bless, M. Uhlmann, J. Schiffmann, S.S. Bertsch, High temperature heat pumps: market overview, state of the art, research status, refrigerants, and application potentials, *Energy* 152 (2018) 985–1010, <https://doi.org/10.1016/j.energy.2018.03.166>.
- [18] E. Shaulsky, Z. Wang, A. Deshmukh, V. Karanikola, M. Elimelech, Membrane distillation assisted by heat pump for improved desalination energy efficiency, *Desalination* (2020), 114694, <https://doi.org/10.1016/j.desal.2020.114694>.
- [19] A.T. Diaby, P. Byrne, P. Loulergue, B. Balanec, A. Szymczyk, T. Maré, O. Sow, Design study of the coupling of an air gap membrane distillation unit to an air conditioner, *Desalination* 420 (2017) 308–317, <https://doi.org/10.1016/j.desal.2017.08.001>.
- [20] A. Khalifa, A. Mezghani, H. Alawami, Analysis of integrated membrane distillation-heat pump system for water desalination, *Desalination* 510 (2021), 115087, <https://doi.org/10.1016/j.desal.2021.115087>.
- [21] Kim Kyung-sung, Membrane Filtering Apparatus Using Heat Pump, 2013, <https://doi.org/10.3726/978-3-653-06033-1/5>.
- [22] Ozone Secretariat, Handbook for the Montreal Protocol on Substances That Deplete the Ozone Layer, 14th ed., 2020. <https://ozone.unep.org/sites/default/files/Handbooks/MP-Handbook-2020-English.pdf>.
- [23] J.A. Andrés-Mañas, A. Ruiz-Aguirre, F.G. Acien, G. Zaragoza, Performance increase of membrane distillation pilot scale modules operating in vacuum-enhanced air-gap configuration, *Desalination* 475 (2020), 114202, <https://doi.org/10.1016/j.desal.2019.114202>.
- [24] T. Tong, M. Elimelech, The global rise of zero liquid discharge for wastewater management: drivers, technologies, and future directions, *Environ. Sci. Technol.* 50 (2016) 6846–6855, <https://doi.org/10.1021/acs.est.6b01000>.
- [25] Coolprop, Coolprop, (n.d.). <http://coolprop.org/> (accessed May 7, 2020).
- [26] M. Bindels, N. Brand, B. Nelemans, Modeling of semibatch air gap membrane distillation, *Desalination* 430 (2018), <https://doi.org/10.1016/j.desal.2017.12.036>.
- [27] L. Wang, C. Violet, R.M. Duchanois, M. Elimelech, Derivation of the theoretical minimum energy of separation of desalination processes, *J. Chem. Educ.* 97 (2020) 4361–4369, <https://doi.org/10.1021/acs.jchemed.0c01194>.
- [28] J.H.L. V, J. Swaminathan, H.W. Chung, D.M. Warsinger, Membrane distillation model based on heat exchanger theory and configuration comparison, *Appl. Energy* 184 (2016) 491–505, <https://doi.org/10.1016/j.apenergy.2016.09.090>.
- [29] R.L. Stover, A. Ameglio, P.A.K. Khan, The ghalliah SWRO plant: an overview of the solutions adopted to minimize energy consumption, *Desalination* 184 (2005) 217–221, <https://doi.org/10.1016/j.desal.2005.03.059>.
- [30] A.S. Stillwell, M.E. Webber, Predicting the specific energy consumption of reverse osmosis desalination, *Water (Switzerland)* 8 (2016) 1–19, <https://doi.org/10.3390/w8120601>.
- [31] C. Fritzmann, J. Löwenberg, T. Wintgens, T. Melin, State-of-the-art of reverse osmosis desalination, *Desalination* 216 (2007) 1–76, <https://doi.org/10.1016/j.desal.2006.12.009>.
- [32] A. Ruiz-Aguirre, J.A. Andrés-Mañas, J.M. Fernández-Sevilla, G. Zaragoza, Experimental characterization and optimization of multi-channel spiral wound air gap membrane distillation modules for seawater desalination, *Sep. Purif. Technol.* 205 (2018) 212–222, <https://doi.org/10.1016/j.seppur.2018.05.044>.
- [33] A.A. Atia, N.Y. Yip, V. Fthenakis, Pathways for minimal and zero liquid discharge with enhanced reverse osmosis technologies: module-scale modeling and techno-economic assessment, *Desalination* 509 (2021), 115069, <https://doi.org/10.1016/j.desal.2021.115069>.
- [34] D.M. Davenport, A. Deshmukh, J.R. Werber, M. Elimelech, High-pressure reverse osmosis for energy-efficient hypersaline brine desalination: current status, design considerations, and research needs, *Environ. Sci. Technol. Lett.* 5 (2018) 467–475, <https://doi.org/10.1021/acs.estlett.8b00274>.
- [35] Z. Wang, A. Deshmukh, Y. Du, M. Elimelech, Minimal and zero liquid discharge with reverse osmosis using low-salt-rejection membranes, *Water Res.* 170 (2020), 115317, <https://doi.org/10.1016/j.watres.2019.115317>.